

Multiphoton microscopy for the investigation of dermal penetration of nanoparticle-borne drugs

Frank Stracke^{1,C}, Barbara Weiss², Claus-M. Lehr²,
Karsten König¹, Ulrich F. Schaefer², Marc Schneider²

1) Fraunhofer Institute for Biomedical Technology, Ensheimer Str. 48, 66386 St. Ingbert, Germany

2) Department of Biopharmaceutics & Pharmaceutical Technology, Saarland University, 66123 Saarbrücken, Germany

C) Corresponding author:

eMail: frank.stracke@ibmt.fraunhofer.de, phone / fax: +49 (0)6894 980-166 / -152

Short title: "Multiphoton microscopy of particle penetration"

Abbreviations:

NADH: Nicotineamide adenine	
CLSM: Confocal laser scanning microscopy	dinucleotide, hydrogenated form
DMAP: 1-Ethyl-3-(3-dimethylaminopropyl)-carbodiimide hydrochloride	NIR: Near infrared
FA: Fluoresceinamine	PLGA: Polylactide- <i>co</i> -glycolide
FWHM: Full width half maximum	PMT: Photomultiplier tube
MPM: Multiphoton microscopy	PVA: Polyvinylalcohol
NA: Numerical aperture	ROI : Region of interest
	x, y : lateral dimensions
	z : normal dimension / subsurface depth

This document is a preprint version of :

Multiphoton Microscopy for the Investigation of Dermal Penetration of Nanoparticle-Borne
Drugs

Formal publication in:

Journal of Investigative Dermatology advance online publication 18 May 2006; doi:

10.1038/sj.jid.5700374

Authors:

Frank Stracke, Barbara Weiss, Claus-Michael Lehr, Karsten König, Ulrich F Schaefer and
Marc Schneider

<http://www.nature.com/jid/journal/vaop/ncurrent/abs/5700374a.html>

Abstract

Multiphoton microscopy of a dually fluorescence-labeled model system in excised human skin is employed for high resolution three dimensional visualization in order to study the release, accumulation and penetration properties of drugs released from nanoscale carrier particles in dermal administration. Polymer particles were covalently labeled with fluorescein while Texas Red as a drug-model was dissolved in the particle to be released to the formulation matrix. Single nanoparticles on skin could easily be localized and imaged with diffraction limited resolution. The temporal evolution of the fluorescent drug-model concentration in various skin compartments over more than five hours was investigated by multiphoton spectral imaging of the same area of the specimen. The three dimensional penetration profile of the drug-model in correlation with skin morphology and particle localization information are obtained by a multiple laser line excitation experiment. Multiphoton microscopy combined with spectral imaging was found to allow non invasive long term studies of particle-borne drug-model penetration into the skin with sub cellular resolution. By dual color labeling a clear discrimination between particle-bound and released drug-model was possible. The introduced technique was shown to be a powerful tool in revealing the dermal penetration properties and pathways of drugs and nanoscale drug vehicles on microscopic level.

Introduction

The encapsulation of active substances is a common pharmaceutical strategy to modify the transport and release properties of a drug. Especially to nanoparticulate systems great potential is attributed in the field of drug delivery. This is partly due to the fact, that sensitive drugs can be hidden from degradation in the particles (Daniels, 2006; Volodkin *et al.*, 2004). Further powerful properties of nanoscale drug carrier are the sustained release (Daniels, 2006; El-Samaligy *et al.*, 1986) of the active substances resulting in an extended activity or enhanced uptake (Alvarez-Roman *et al.*, 2004c; Lombardi Borgia *et al.*, 2005) and the possible reduction of adverse effects (Lamprecht *et al.*, 2001). Functional coatings of the particles may allow the targeted accumulation and release of drugs at their therapeutic sites (Dinauer *et al.*, 2005; Kotrotsiou *et al.*, 2005; Wartlick *et al.*, 2004).

Widely used nanoparticle formulations are based on poly(lactic acid) (PLA), poly(glycolic acid) (PGA), and their co-polymers, poly(lactide-*co*-glycolide) (PLGA), which are known for their good biocompatibility and degradability through natural pathways (Brannon-Peppas, 1995). In oral and parenteral applications these solid biodegradable polymeric nanoparticle have already shown their advantage over liposomes by their increased stability (Hans and Lowman, 2002; Ravi Kumar *et al.*, 2003; Soppimath *et al.*, 2001). Nanoscale polymeric drug vehicles have also been proposed for transdermal delivery (Alvarez-Roman *et al.*, 2004c; Kohli and Alpar, 2004; Lombardi Borgia *et al.*, 2005; Luengo *et al.*, accepted). Penetration (Alvarez-Roman *et al.*, 2004c; Luengo *et al.*, accepted), permeation (Luengo *et al.*, accepted) and accumulation (Toll *et al.*, 2004) of some particle-borne drugs and drug models after topical application have been investigated by conventional techniques and confocal microscopy of single stained particles.

Established methods for the investigation of drug penetration into the skin are mostly destructive: a representative sample of a defined skin layer is isolated and extracted for

chemical analysis (tape stripping method, cryo-sectioning) (Brain *et al.*, 2002; Wagner *et al.*, 2001). The result of such an experiment is an area averaged depth profile of the drug in the skin to a certain time (Luengo *et al.*, accepted). The depth profiles for different incubation times have to be investigated with different samples, neglecting the individual characteristics of biological specimens. To evaluate and optimize novel dermal drug delivery strategies using nanoscale drug carriers, more versatile techniques are required. Such a technique must allow the discrimination between free and carrier-bound drug, the tracing of the carrier nanoparticles, the allocation of microscopic delivery pathways to specific dermal sites and time studies on the same skin area. After application of nanoparticles as topical vehicles one can imagine different routes of drug delivery. It could be assumed that the whole nanoparticulate system is taken up without being destroyed (Kohli and Alpar, 2004) or that the nano-carrier is decomposed close to the skin surface and thereafter the active substance penetrates in dependence on the local environment (acidification or absorption of drug / nanoparticle-complexes) as speculated in Luengo *et al.* for the enhanced long term uptake of flufenamic acid (Luengo *et al.*, accepted). Furthermore, a direct diffusion from the carrier into the stratum corneum is reasonable as described by Bouwstra *et al.* (Meuwissen *et al.*, 1998; Van Kuijk-Meuwissen *et al.*, 1998a). In any case, it is essential to distinguish between particles, particle-bound drug and released drug. Herein we describe how multiphoton laser scanning microscopy (MPM) and confocal laser scanning microscopy (CLSM) can be very beneficial tools in order to meet all these demands in one experiment. In particular multiphoton microscopy enables repeated non-invasive investigations of skin tissue down to the dermis with virtually no out-of-focus effects of the scanning laser beam (Konig and Riemann, 2003). Due to multiple labeling techniques in combination with multiphoton spectral imaging or selective excitation of the labels a clear discrimination between particle and free drug model is possible, as well as tracking of single particles. Due to the excitation of endogenous fluorophores of the skin by multiphoton excitation and the correlation of the

resulting autofluorescence image to the drug fluorescence pattern the identification of accumulative spots and penetration pathways is possible with sub-cellular resolution (Yu *et al.*, 2003; Yu *et al.*, 2002). Multiphoton microscopy provides several considerable advantages over conventional fluorescence and confocal microscopy (Konig, 2000; Xu *et al.*, 1996). Three of which are relevant to the present investigation: the concentration of all light-matter interactions to the focal volume, the convenient separation of fluorescence from scattered excitation light due to the large blue-shift of fluorescence and the capability to excite compounds which else require ultraviolet excitation, in particular native fluorophores as NADH and keratin (Huang *et al.*, 2002; Konig and Riemann, 2003; Pena *et al.*, 2005). The confined interaction volume at the focal point is due to the I^n -dependence of n-photon absorption processes on the illumination intensity I . Hence already two-photon absorptions are confined to a sub-femtoliter focal volume, in which the illumination intensity is sufficiently high. Since the excitation with near infrared (NIR) lasers matches the optical window of biological matter (700 – 1100 nm) virtually no single-photon absorptions occur in the illumination cones. As a consequence, no fluorescence is generated outside the focal volume and therefore three dimensional spatial resolution is an inherent feature of multiphoton laser scanning microscopy. Furthermore out of focus photo-damage is drastically reduced and light penetration depth into tissue is significantly enhanced (Centonze and White, 1998; Konig and Riemann, 2003).

Since most pharmaceutical substances are basically non fluorescent, the usage of appropriate fluorescent model compounds is reasonable. Such a model compound has to match the molecular size, charge, membrane permeability, distribution, and diffusion coefficients as good as possible. A fluorescent label fixed to the actual drug molecule changes these properties and thus the penetration behavior considerably. Hence labeling only makes sense if specific interactions of the drug to certain sites are investigated. In contrast the non-superficial fluorescent labeling of the nanoscale carrier particles doesn't change the particle's

pharmacokinetics significantly. In addition, the fate of the nano-carrier itself and its role in the changed uptake behavior may be investigated. In this work a two color labeling technique was used to trace the migration of the nanoparticles and to observe the release and uptake of the drug-model compound. To this end fluoresceinamine was covalently linked to the polymeric particle material and Texas Red was physically resolved in the particle matrix. It is shown, that individual sub-diffraction sized nanoparticles can be localized, traced and spectrally analyzed. Due to the two-color staining a clear discrimination between free and particle-bound dye was achieved. The method turned out to allow stable measurements on excised human skin over hours with no significant drift of the specimen.

Results

Multiphoton fluorescence imaging

The multiphoton optical sections were recorded from the skin surface down to the bottom of the shown dermatoglyph at $z = 42 \mu\text{m}$ over five hours under identical conditions (Figure 1). It was found, that the sub-diffraction-limit sized particles can easily be detected and localized, as long as their mean distance is well above this limit. They appear as lateral diffraction limited spots with widths of about $0.5 \mu\text{m}$, which is in reasonable agreement with theoretical predictions for the minimum achievable full width half maximum FWHM of 302 nm ¹. A typical fluorescence profile of two particles *in situ* is displayed in Figure 2. The minimal fluorescence spot size may be broadened by Brownian motion and distorted by flux motions of the gel in the dermatoglyphs. In case of the bright spots the detector went into saturation, which additionally caused a considerable broadening of the spot size. The mean distance between the nanoparticles in the present formulation is on the order of $5 \mu\text{m}$. Three dimensional tracing of individual particles is easily possible under the outlined conditions and allows detailed studies on the migration of nanoscale drug carriers in the skin.

The significant endogenous fluorescence of keratin under two-photon excitation enables imaging of the outermost layer of the stratum corneum and hence the dermal topography. The PLGA particles are obviously not able to penetrate the stratum corneum and stay in the gel-filled dermatoglyphs over the entire observation time (Figure 3). This corresponds with former findings of the authors in which no penetration of PLGA particles loaded with flufenamic acid into the human skin could be observed (Luengo *et al.*, accepted).

¹ *The theoretical FWHM was calculated by convolution of a sphere profile of $d = 290 \text{ nm}$ with the squared intensity point spread function IPSF². The ISPF² was derived according (Zipfel *et al.* 2003).*

It is noteworthy, that even after more than five hours swelling, shrinking and stress relaxation motions of the skin sample only lead to minute deformations within the field of view. No drift of the specimen occurred.

No significant changes in the background fluorescence intensity of the ointment matrix or in the stratum corneum as a consequence of the Texas Red release and accumulation were observed in the multiphoton fluorescence mode. The reason for this finding is the comparable low two-photon absorption cross-section of Texas Red at $\lambda = 800$ nm (Figure 4) while fluorescein and keratin are efficiently excited.

Multiphoton spectral imaging

In order to investigate the distribution of the drug-model Texas Red as a function of time, two-photon spectral imaging was applied. In this technique the luminescence signal from the specimen is spectrally resolved and the spectrum is stored for each pixel or voxel, respectively. From these data, fluorescence spectra for arbitrary regions of interest can be calculated. The laser wavelength of 800 nm leads to an image which is dominated by the fluorescein emission and the endogenous fluorescence of the stratum corneum. But due to the different sensitivity spectrum of the META detector array the sensitivity loss in the red spectral range is less drastic compared to the PMTs. Even faint contributions of the Texas Red fluorescence to any pixel or region of interest (ROI) of the image can now be isolated from the other emissions by spectral separation. In the present study a $145 \times 145 \mu\text{m}^2$ area from the middle of Figure 3 was investigated. The spectral images were recorded to similar times as the optical sections. In Figure 5a a typical example of such a spectral image is displayed in true color mode. The nanoparticles appear clearly green, indicating that their fluorescence originates predominantly from the covalently bound fluorescein. The outermost layer of the stratum corneum shows a heterogeneous distribution of colors. For an interpretation the

fluorescence spectrum of the respective region is taken (Figure 6a, ROI 2). The reddish color of the deeper skin is mainly caused by residual scattered excitation light beyond 700 nm (Figure 6a, ROI 3).

Three regions of interest are indicated in Figure 5a: ROI 1 contains the gel matrix including the nanoparticles, ROI 2 contains the keratinous surface layer of the stratum corneum and ROI 3 covers the deeper layers down to approximately 20 μm . Average fluorescence spectra are calculated from the ROIs at different times to reveal the evolution of the Texas Red concentration in these regions. Due to the small deformations of the specimen, especially in vertical direction, the ROIs do not enclose exactly identical skin domain at the different times. This may be a cause for small discrepancies in the spectral analysis. But since the ROIs were always chosen to enclose only skin compartments according to the definitions above, the spectral analysis will still reveal the accurate trends. To rule out errors due to varying offsets and fluctuations in the absolute signal, the Texas Red fluorescence is determined relative to an emission, which is expected to be constant in time. For ROI 1 the fluorescein emission from the nanoparticles at 525 nm is used, for ROI 2 the keratin autofluorescence around 510 nm and for ROI 3 the back scattered excitation light at 714 nm. Linear baselines are applied to reduce the influence of the background (Figure 6a). Since in particular the autofluorescence in ROI 2 and the Texas Red emission in ROI 3 show only dim intensities, the determined intensity ratios for ROI 2 and ROI 3 have large uncertainties. Anyway the rough trends are visible in those plots.

Whereas the Texas Red content in the nanoparticles showed up to be low and basically constant already from the first measurement at $t = 30$ minutes (Figure 5c), the concentration of Texas Red in the gel matrix drops significantly with time (Figure 5b, 7b). The Texas Red concentration in the superficial layer of the stratum corneum is also declining, but less rapid (Figure 6c). The observation of declining concentration in this compartment from the earliest measurement at $t = 30$ minutes on means, that the vast fraction of Texas Red

was taken up from the gel to the stratum corneum surface almost immediately after application. Furthermore the release of Texas Red from the nanoparticles to the matrix started well before application to the skin. Probably the predominant fraction was released to the solvent even before suspension of the particles to the hydrogel. Since the concentration of the released dye is decreasing in the gel-filled dermatoglyphs and in the stratum corneum surface it must have penetrated the skin (or metabolism of the dye occurred, which is unlikely). In fact an increase of Texas Red concentration in the deeper stratum corneum and stratum granulosum is evident (Figure 6d), indicating a slow penetration of the dye. The fits to the plots are mono-exponential decays and growth, respectively. The fit curves have no theoretical pharmacokinetic background, but allow a convenient comparison of decay and rise times. Advanced interpretations of the release, uptake and penetration of the dye will be possible only on the basis of an appropriate pharmacokinetic model. The decay times of the mono-exponential fits are $\tau_{ROI 1} = 35 \pm 6$ minutes, $\tau_{ROI 2} = 148 \pm 319$ minutes and the rise time is $\tau_{ROI 3} = 59 \pm 38$ minutes.

Multitracking studies

After 320 minutes a multitracking experiment visualizes the distribution of Texas Red, fluorescein and keratin fluorescence (Figure 7). In this technique the signals from the different fluorophores are separated by their excitation spectra, not by their fluorescence spectra as done in spectral imaging. As opposed to the spectral images, which are recorded with one excitation wavelength, herein the successive use of three excitation sources may lead to small mismatches between the channels. The vertical mismatch of the NIR two-photon excitation image to the images excited by visible laser sources is due to chromatic aberrations of the objective. The small average lateral shift from the fluorescein image, excited by the 488 nm argon ion laser line, to the Texas Red image, excited by the 543 nm helium neon laser

line, is due to the microscope optics and could be compensated by image processing. Furthermore a multitracking experiment yields an overlay of successive scan images. If the specimen shows dynamics, any motion is reflected by shifts from one scan to the next. One must keep these mismatches in mind when performing colocalisation studies on different dyes. In Figure 7d an average lateral shift of about 6 μ m is evident between the fluorescein image and the Texas Red image. The shift is not uniform for all particles, but varies due to flux motions within the hydrogel during the acquisition times of the three single images of the multitracking experiment. The particle pattern in the two-photon excited image exhibits no correlation with the visibly excited images, indicating a vertical mismatch of the focal planes exceeding the normal size of the focal volumes (approximately 1 μ m). This mismatch is also evident in the missing congruency of the dermatoglyph borders in the two-photon excited image and the 543 nm excited image (Figure 7). The keratin autofluorescence seems to be located not at the surface of the Texas Red stained dermatoglyph, but some microns inside of the skin. This is a consequence of the vertical mismatch between the NIR and visible focus. Nevertheless detailed distribution analysis for each isolated dye can be performed as well as a rough colocalisation study, since fluorescein and keratin are not excited by the 543 nm laser line and Texas Red is virtually exclusively excited by this excitation source (Figure 4).

The 488 nm excited image (green) proves, that fluoresceinamine is strictly bound to the particles and not released during the time of observation. Previous experiments showed that released fluorescein is rapidly bound to the keratinous layer of the stratum corneum. In the present study no such accumulation is found. The fluorescence spots of the particles are mostly broadened due to saturation. In the 543 nm excited images (orange) the distribution of Texas Red is visible. The predominant fraction of the dye is to be found within the skin, but the particles are also slightly observable. Obviously there is still a certain amount of the dye stored in the nanoparticles, though the release process has proceeded far. The released Texas Red penetrated the skin and accumulated in the stratum corneum down to approximately

20 μm (Figure 7b). In Figure 7c, recorded at a depth of 32 μm , the penetration into deeper skin compartments can be recognized, since the walls of the dermatoglyph are steep enough to reveal the diffusion from the superficial layers inwards. The distribution of Texas Red in the skin is not uniform, but structured. It is conspicuous, that the superficial accumulation is strongest, where the skin adjoins to large gel-filled spaces. Beneath the superficial layer the distribution of the drug-model is more uniform, which indicates faster diffusion of the compound in these skin compartments. The fundamental discrepancy between the visible excited images and the two-photon image proves that the skin visible structures from the two-photon image are predominantly due to keratin autofluorescence and not due to the superficial accumulation of Texas Red. xz-sections can be extracted from the multitracking z-stacks, which nicely exhibit the concentration profile in normal direction (Figure 8). The highest concentrations of Texas Red in the deeper layers are found under superficial areas with pronounced keratin autofluorescence. This supports the hypothesis of a fast resorption of Texas Red from the hydrogel to the keratinous compartments and a slower diffusion from there to the skin tissue underneath. A vertical mismatch of several microns between the 543 nm excited Texas Red fluorescence and the multiphoton excited endogenous keratin fluorescence due to the chromatic aberration of the optics is apparent in all xz-sections.

Discussion

A major challenge in the design of nanoscale drug delivery entities is the development of mechanisms which triggers the release of the drug when the nanoparticle attains its therapeutic site. For dermal applications such mechanisms may consist of an intrinsic recognition element for specific sites or compounds of the skin and a thereby controlled release step. Another approach to this end is to modify the particle surface in a way that they accumulate at the therapeutic site and to start the drug release by external stimuli

like light illumination or the delayed application of a kick-off agent. A pure diffusive release of a drug from suspended particles starts at the moment of suspension and after a certain storage time the drug is predominantly dissolved in the suspension matrix. Hence this way of formulation compromises all advantages of nano particular drug delivery. Since so far no such intelligent trigger techniques are established for topical application of nanoscale drug carriers, the simple diffusive release mechanism is observed in the present work to demonstrate the capabilities of laser scanning microscopy in this field. As a consequence it was found, that the major fraction of Texas Red was already released to the gel matrix at the moment of the first measurement. This observation demonstrates that diffusive release of drugs from the particle cannot be employed for the practical use of nanoscale drug carriers and in general stresses the need for the design of intelligent nano carriers with controllable release behavior. The three dimensional microscopic and spectral resolution of the utilized techniques showed up to have a more versatile potential for the evaluation of such smart nanoparticle formulations than conventional penetration study methods.

In general, multiphoton and confocal microscopy of dually labeled nanoparticles in human skin biopsies have been demonstrated to be very suitable techniques to investigate the migration, accumulation, release and penetration of nanoparticle-borne drugs in dermal application. By different fluorescence spectra of the covalently fixed and the physically dissolved dye discrimination between particle-bound and released compounds is possible. By performing spectral imaging the quantitative analysis of the release process is much less interfered by background emissions and crosstalk errors than in a conventional two detector channel study with a dichroic beamsplitter. Furthermore an emission can be attributed to a certain compound with a high degree of accuracy by resolving the fluorescence spectrum.

It was shown, that tracing of even single particles of about 300 nm diameter in the gel matrix inside the dermatoglyphs is not a difficult task. The observation depth of multiphoton microscopy even in turbid media is on the order of several hundred microns

(Centonze and White, 1998) and is mostly limited by the working distance of the applied high numerical aperture objectives. Hence single fluorescent nanoparticles should be observable within the skin down to the dermis. This is of particular importance if particles are investigated, which are able to penetrate the epidermal layers. No penetration of particles into the skin was found in the present study. Due to the three dimensional sub cellular resolution and the possibility of repeated non-invasive investigations of the same skin area detailed information on the penetration pathway of particle-bound and free drug-models are accessible.

Since confocal microscopy with visible excitation does not provide such enhanced observation depths, the multitracking technique is primarily adequate for investigations on the upper skin layers. Problems may arise from possible lateral mismatches, the chromatic shift of the focal planes in case of strongly differing excitation wavelengths and the time lag between the single scans. The influences of these interferences have to be carefully regarded in the interpretations of multitracking studies. Nevertheless it can be a powerful tool if the applied fluorophores are basically excited exclusively by the chosen laser lines, as demonstrated in the present study.

The specimen mounting fulfilled the objectives of keeping the skin sample in place with an accuracy of few microns in three dimensions, to avoid desiccation and to minimize swelling and shrinking effects. In the present study excised, frozen and thawed human skin was used. The properties of a skin specimen treated accordingly will certainly differ from skin *in vivo* and freshly excised biopsies, as e.g. the pH depth profile changes rapidly after excision (Wagner *et al.*, 2003) and the endogenous NADH fluorescence of the vital epidermal layers is virtually vanished after frozen storage. In spite of these physiological changes permeation measurements did not exhibit a changed passage behavior for the investigated compounds after frozen storage of human skin, indicating that the non vital superficial layer of the stratum corneum was the main penetration barrier (Wagner *et al.*, 2004). A multiphoton microscopy

experiment on freshly excised human skin or *in vivo* could reveal even more detailed information on the drug penetration into the vital skin layers, since the cellular autofluorescence would allow the allocation of the drug pathways on single cell level.

By deliberate variation of the fluorescent drug-model, correlations of the microscopic penetration behavior with various physicochemical properties of the drug-models could be investigated. An intelligent release mechanism providing for a defined initial time of release from the nanoscale drug carrier would allow to study the accurate evolution of drug concentrations in the diverse skin compartments and to derive a pharmacokinetic model of the drug uptake from nano particular formulations.

Concluding, we demonstrated the benefits of multi-color labeling of biodegradable nanoparticles and the intriguing insights into the penetration behavior of particle-borne drugs due to the combination with multiphoton microscopy and confocal laser scanning microscopy. The usage of two fluorescent dyes of well separated absorption and emission spectra enabled the investigation of the transport of a fluorescent drug model *in situ*. This might be extended to multiple loading of nanoparticles with two or more drug models which differ in spectral and physicochemical properties for direct comparison. Furthermore relevant pharmaceutical compounds with native fluorescence may be investigated as well as intelligent release mechanisms. The kinetics of the drug transport from the initial formulation to the subcutaneous compartments can be studied in elementary steps, as the enrichment of particles in certain dermal sites (Toll *et al.*, 2004), the release of the drug from the particles, its uptake into the stratum corneum, the diffusion into the deeper skin layers etc.. The determination of the enrichment in dependence of time as well as the visualization of the ‘structured’ diffusion process into the skin envisages the potential of this approach. In addition, the covalent label to the nanoparticle itself enables the investigator to follow the fate of the nano-carrier, its uptake, accumulation or decomposition. This might be very meaningful in particular for the exploration of the penetration function of hair shafts. First evidence was observed that these

follicles might play an important role (Alvarez-Roman *et al.*, 2004b; Toll *et al.*, 2004; Van Kuijk-Meuwissen *et al.*, 1998b).

Methods & Material

Materials:

Poly(L-lactide-*co*-glycolide) (PLGA) (Resomer RG 50:50 H) was kindly provided by Boehringer Ingelheim (Boehringer Ingelheim GmbH & Co. KG, Ingelheim, Germany). 5-Fluoresceinamine (FA) and 1-ethyl-3-(3-Dimethylaminopropyl)-carbodiimide hydrochloride (DMAP) were obtained from Sigma (Sigma Chemical Co., St. Louis, MO, USA). Polyvinylalcohol (PVA) (Mowiol 4-88) was purchased from Kuraray (Kuraray Specialities GmbH, Frankfurt am Main, Germany). Texas Red[®] was provided by Atto-Tec (Atto-Tec GmbH, Siegen, Germany). We grateful acknowledge the kind provision of Natrosol[®] 250 M hydrogel (Aqualon, Hercules Inc., DE, USA) by J. Luengo. All other chemicals are of analytical grade.

Polymer labeling and preparation of dual color nanoparticles

FA bound PLGA (FA-PLGA) was prepared based upon the method described by Horisawa et al. (Horisawa *et al.*, 2002). Briefly, PLGA (3.07g) and FA (0.0583g) were dissolved entirely in 30ml of acetonitrile with 0.0408g of DMAP and incubated at room temperature for 24h under light protection and gentle stirring. The resultant FA-PLGA was precipitated by the addition of purified water and separated by centrifugation. The polymer was rinsed from excessive reagents (dissolution in acetone and precipitation with ethanol in terms) and then lyophilized (Alpha 2-4 LSC, Martin Christ Gefriertrocknungsanlagen GmbH, Osterode Germany).

Texas Red nanoparticles were prepared from FA-PLGA employing a single emulsion method (oil in water). The emulsion was formed between an organic FA-PLGA solution (2%

(w/v) in ethyl acetate) which additionally contained 30µl of a saturated Texas Red solution and 5ml of a PVA solution (1% in demineralized water) under stirring on a magnetic stirrer for 2h. Then, the emulsion was homogenized using an Ultra-Turrax[®] T 25 Mixer (Janke und Kunkel GmbH & Co., Staufen, Germany) at 13,500rpm and the organic solvent was removed by a rotary evaporator. The mean particle size was determined to $d = 290 \pm 5$ nm using photocorrelation spectroscopy (Zetasizer[®]3000HSA, Malvern Instruments GmbH, Herrenberg, Germany) and the homogeneity of the particles was verified using scanning probe microscopy (BioScope, Veeco, Santa Barbara, USA) (Figure 9). To prepare the nanoparticle ointment a Natrosol[®] gel (3% w/w) was mixed with an aqueous suspension of the nanoparticles in a 1:1 ratio.

Skin preparation:

Excised human skin from Caucasian female patients, who had undergone abdominal plastic surgery, was used. The procedure was approved by the Ethical Committee of the Caritas-Traegergesellschaft, Trier, Germany (6th July 1998). Adequate health and no medical history of dermatological disease were required. After excision the skin was cut into 10×10 cm² pieces and the subcutaneous fatty tissue was removed from the skin specimen using a scalpel. Afterwards the surface of each specimen was cleaned with water, wrapped in aluminum foil and stored in polyethylene bags at -26°C until use. Previous investigations have shown that no change in the penetration characteristics occurs during the storage time of 6 months (Bronaugh *et al.*, 1986; Wagner *et al.*, 2004).

Laser Scanning Microscopy:

The microscopy studies were performed on a versatile laser scanning microscope (LSM 510 NLO META, Carl Zeiss Jena GmbH, Germany) for conventional confocal

microscopy with multiple excitation laser lines and multiphoton excitation microscopy. Herein, the 488 nm laser line of the internal argon ion laser and the 543 nm line of the internal helium neon laser were applied for confocal imaging. For multiphoton microscopy a femtosecond pulsed titan:sapphire laser at $\lambda = 800$ nm with 90 fs pulse width and 80 MHz repetition rate (Coherent Vitesse) was coupled into the microscope.

The META scanning and detection module offers different ways to detect the fluorescence light. First, the complete emission is distributed between two sensitive photomultiplier tubes (PMT) by means of neutral and dichroic mirrors. Second, the emission signal is spectrally dispersed by a diffraction grating and guided on a 32 channel photomultiplier array for spectral analysis. Each channel detects a spectral range of about 10nm in this arrangement. Three different imaging modes were applied in the present study: (a) the multiphoton fluorescence mode for the cumulative detection of the emitted fluorescence. Here the fluorescence intensity is recorded by one PMT. The laser line is blocked by a 650 nm shortpass beamsplitter and a 685 nm shortpass filter. This detection mode is the most sensitive one, but any spectral information is lost. (b) In the multiphoton spectral imaging mode the emitted light is separated from the laser line by the 650 nm shortpass beamsplitter and recorded spectrally resolved by means of the grating and the detector array. Each pixel of a spectral image contains the data of the 32 detector channels, so that emission spectra for each pixel or for defined areas of the image are accessible. The displayed images are true color coded. The spectral data is converted into appropriate RGB values. (c) The multitracking mode is actually an overlay of three fluorescence intensity images, subsequently acquired at different excitation wavelengths. An overlay procedure with two visible excitation laser lines was utilized on similar specimens by Alvarez-Roman et al. (Alvarez-Roman *et al.*, 2004a). The excitation wavelengths are chosen to be preferably absorbed by exclusively one fluorophore (Figure 4). The 488nm argon ion laser line is predominantly absorbed by fluorescein, the 543 nm helium neon laser line by Texas Red

exclusively. Two-photon excitation at 800 nm is strong for fluorescein and the endogenous fluorophore keratin, but poor for Texas Red.

Two-photon excitation spectra (Figure 4) were acquired according to a modified 'excitation fingerprinting' procedure introduced by Dickinson et al. (Dickinson *et al.*, 2003). In contrast to the excitation fingerprinting technique, where the excitation power is kept constant for different wavelengths, herein the laser power calibration is adjusted for constant photon flux at different wavelengths to yield correct two-photon excitation spectra (Schneider *et al.*, 2005). One-photon excitation and fluorescence spectra were acquired with a Hitachi FL 4500 fluorometer using 50 μ M aqueous solutions of fluorescein isothiocyanate (FITC) dextran and Texas Red. FITC dextran was used in order to investigate a compound preferably akin to FA-PLGA while showing good water solubility. The spectral properties of the fluorescein derivatives are almost unaffected by different substituents in the 5-position.

Sample preparation

For microscopy, disks of 0.8 cm diameter were punched out of frozen skin and placed surface-up on a microscopy slide inside a circular vertical spacer. After application of the ointment to the skin surface a cover slide was fixed onto the spacer by double-faced adhesive tape in a way that the skin surface was gently pressed against the cover slide. This setup provides constant specimen thickness and prevents desiccation of the skin sample. The observation was performed through the cover slide by means of a 40 \times /1.3 NA Oil Objective (Plan Neofluar, Carl Zeiss Jena GmbH, Germany).

Acknowledgements

This work is part of the PhD thesis of Ms. Barbara Weiss. We grateful acknowledge the kind provision of Natrosol[®] hydrogel by J. Luengo and the supply of excised human skin samples by K.-H. Kostka (Department of Plastic and Hand Surgery, Caritaskrankenhaus, Lebach, Germany).

References

- Alvarez-Roman R, Naik A, Kalia Y, Guy RH and Fessi H (2004a). Skin penetration and distribution of polymeric nanoparticles. *Journal of Controlled Release* **99**:53-62.
- Alvarez-Roman R, Naik A, Kalia YN, Fessi H and Guy RH (2004b). Visualization of skin penetration using confocal laser scanning microscopy. *European Journal of Pharmaceutics and Biopharmaceutics* **58**:301-316.
- Alvarez-Roman R, Naik A, Kalia YN, Guy RH and Fessi H (2004c). Enhancement of topical delivery from biodegradable nanoparticles. *Pharmaceutical Research* **21**:1818-1825.
- Brain KR, Walters KA and Watkinson AC: Methods for Studying Percutaneous Absorption, Walters KA (ed): Dermatological and Transdermal Formulations 1st ed., pp 197 (Marcel Dekker Inc., New York 2002).
- Brannon-Peppas L (1995). Recent advances on the use of biodegradable microparticles and nanoparticles in controlled drug delivery. *International Journal of Pharmaceutics* **116**:1-9.
- Bronaugh RL, Stewart RF and Simon M (1986). Methods for Invitro Percutaneous-Absorption Studies. VII. Use of Excised Human-Skin. *J Pharm Sci* **75**:1094-1097.
- Centonze VE and White JG (1998). Multiphoton Excitation Provides Optical Sections from Deeper within Scattering Specimens than Confocal Imaging. *Biophys J* **75**:2015-2024.
- Daniels J (2006). How polymeric microspheres deliver the goods. *Pharmaceutical Technology Europe* **18**:30-32.

- Dickinson ME, Waters CW, Fraser SE, Simbuerger E and Zimmermann B (2003). Multiphoton excitation spectra in biological samples. *Journal of Biomedical Optics* **8**:329-338.
- Dinauer N, Von Briesen H, Balthasar S, Weber C, Kreuter J and Langer K (2005). Selective targeting of antibody-conjugated nanoparticles to leukemic cells and primary T-lymphocytes. *Biomaterials* **26**:5898-5906.
- El-Samaligy MS, Rohdewald P and Mahmoud HA (1986). Polyalkyl cyanoacrylate nanocapsules. *Journal of Pharmacy and Pharmacology* **38**:216-218.
- Hans ML and Lowman AM (2002). Biodegradable nanoparticles for drug delivery and targeting. *Current Opinion in Solid State & Materials Science* **6**:319-327.
- Horisawa E, Kubota K, Tuboi I, Sato K, Yamamoto H, Takeuchi H et al. (2002). Size-dependency of DL-lactide/glycolide copolymer particulates for intra-articular delivery system on phagocytosis in rat synovium. *Pharmaceutical Research* **19**:132-139.
- Huang SH, Heikal AA and Webb WW (2002). Two-photon fluorescence spectroscopy and microscopy of NAD(P)H and flavoprotein. *Biophys J* **82**:2811-2825.
- Kohli AK and Alpar HO (2004). Potential use of nanoparticles for transcutaneous vaccine delivery: Effect of particle size and charge. *International Journal of Pharmaceutics* **275**:13-17.
- Konig K (2000). Multiphoton microscopy in life sciences. *J Microsc* **200**:83-104.
- Konig K and Riemann I (2003). High-resolution multiphoton tomography of human skin with subcellular spatial resolution and picosecond time resolution. *Journal of Biomedical Optics* **8**:432-439.
- Kotrotsiou O, Kotti K, Dini E, Kammona O and Kiparissides C (2005). Nanostructured materials for selective recognition and targeted drug delivery. *Journal of Physics: Conference Series* **10**:281-284.

- Lamprecht A, Ubrich N, Yamamoto H, Schaefer UF, Takeuchi H, Maincent P et al. (2001). Biodegradable Nanoparticles for Targeted Drug Delivery in Treatment of Inflammatory Bowel Disease. *The Journal of Pharmacology and Experimental Therapeutics* **299**:775-7781.
- Lombardi Borgia S, Regehly M, Sivaramakrishnan R, Mehnert W, Korting HC, Danker K et al. (2005). Lipid nanoparticles for skin penetration enhancement--correlation to drug localization within the particle matrix as determined by fluorescence and parelectric spectroscopy. *Journal of Controlled Release* **110**:151-163.
- Luengo J, Weiss B, Schneider M, Ehlers A, Stracke F, Koenig K et al. (accepted). Influence of nanoencapsulation on human skin transport of flufenamic acid. *Skin Pharmacology and Physiology*.
- Meuwissen MEMJ, Junginger HE, Bouwstra JA, Janssen J and Cullander C (1998). A cross-section device to improve visualization of fluorescent probe penetration into the skin by confocal laser scanning microscopy. *Pharmaceutical Research* **15**:352-356.
- Pena AM, Strupler M, Boulesteix T, Godeau G and Schanne-Klein MC (2005). Spectroscopic analysis of keratin endogenous signal for skin multiphoton microscopy: erratum (vol 13, pg 6268, 2005). *Opt Express* **13**:6667-6667.
- Ravi Kumar MNV, Sameti M, Kneuer C, Lamprecht A and Lehr C-M: Polymeric nanoparticles for drug and gene delivery, Nalwa HS (ed): Encyclopedia of Nanoscience and Nanotechnology, pp 1-19 (American Scientific Publishers, 2003).
- Schneider M, Barozzi S, Testa I, Faretta M and Diaspro A (2005). Two-photon activation and excitation properties of PA-GFP in the 720-920 nm region. *Biophys J* **89**:1346-1352.

- Soppimath KS, Aminabhavi TM, Kulkarni AR and Rudzinski WE (2001). Biodegradable polymeric nanoparticles as drug delivery devices. *Journal of Controlled Release* **70**:1-20.
- Toll R, Jacobi U, Richter H, Lademann J, Schaefer H and Blume-Peytavi U (2004). Penetration profile of microspheres in follicular targeting of terminal hair follicles. *Journal of Investigative Dermatology* **123**:168-176.
- Van Kuijk-Meuwissen MEMJ, Junginger HE and Bouwstra JA (1998a). Interactions between liposomes and human skin in vitro, a confocal laser scanning microscopy study. *Biochimica et Biophysica Acta - Biomembranes* **1371**:31-39.
- Van Kuijk-Meuwissen MEMJ, Mougin L, Junginger HE and Bouwstra JA (1998b). Application of vesicles to rat skin in vivo: A confocal laser scanning microscopy study. *Journal of Controlled Release* **56**:189-196.
- Volodkin DV, Sukhorukov GB and Larionova NI (2004). Protein encapsulation via porous CaCO₃ microparticles templating. *Biomacromolecules* **5**:1962-1972.
- Wagner H, Kostka K-H, Lehr C-M and Schaefer UF (2001). Interrelation of permeation and penetration parameters obtained from in vitro experiments with human skin and skin equivalents. *Journal of Controlled Release* **75**:283-295.
- Wagner H, Lehr C-M, Schaefer UF and Kostka K-H (2003). pH profiles in human skin: Influence of two in vitro test systems for drug delivery testing. *European Journal of Pharmaceutics and Biopharmaceutics* **55**:57-65.
- Wagner H, Schaefer UF, Kostka K-H and Adelhardt W (2004). Effects of various vehicles on the penetration of flufenamic acid into human skin. *European Journal of Pharmaceutics and Biopharmaceutics* **58**:121-129.
- Wartlick H, Michaelis K, Balthasar S, Kreuter J, Langer K and Strebhardt K (2004). Highly specific HER2-mediated cellular uptake of antibody-modified nanoparticles in tumour cells. *Journal of Drug Targeting* **12**:461-471.

- Xu C, Zipfel W, Shear JB, Williams RM and Webb WW (1996). Multiphoton fluorescence excitation: New spectral windows for biological nonlinear microscopy. *Proc Natl Acad Sci U S A* **93**:10763-10768.
- Yu B, Blankschtein D, Langer R, Kim KH and So PTC (2003). Visualization of oleic acid-induced transdermal diffusion pathways using two-photon fluorescence microscopy. *Journal of Investigative Dermatology* **120**:448-455.
- Yu B, Kim KH, So PTC, Blankschtein D and Langer R (2002). Topographic heterogeneity in transdermal transport revealed by high-speed two-photon microscopy: Determination of representative skin sample sizes. *Journal of Investigative Dermatology* **118**:1085-1088.
- Zipfel WR, Williams RM and Webb WW (2003). Nonlinear magic: Multiphoton microscopy in the biosciences. *Nature Biotechnology* **21**:1369-1377.

Figure Captions

Figure 1: $325 \times 325 \mu\text{m}^2$ multiphoton optical sections of human skin treated with a hydrogel suspension of two color labeled nanoparticles. The sub-surface depths of the displayed images are (a) $-6\mu\text{m}$, (b) $-9\mu\text{m}$, (c) $-12\mu\text{m}$, (d) $-15\mu\text{m}$, (e) $-24\mu\text{m}$, (f) $-33\mu\text{m}$. The keratin autofluorescence clearly shows the surface of the dermatoglyphs. The excitation power for the multiphoton optical sections was $P_{\text{EX}} = 5 \text{ mW}$, the pixel acquisition time $t_{\text{px}} = 3.2 \mu\text{s}$.

Figure 2: Fluorescence intensity profile of two multiphoton excited nanoparticles *in situ*. The bimodal fit yields a full width at half maximum (FWHM) of $0.5\mu\text{m}$. This is a reasonable value for the diffraction limited resolution of nanoscale particles under the present conditions.

Figure 3: $325 \times 325 \mu\text{m}^2$ multiphoton optical sections at a depth of $-27\mu\text{m}$ 15, 50 and 315 minutes after application of the nanoparticular formulation.

Figure 4: One- (solid line) and two-photon (open circles plus B-spline fit) excitation spectra are displayed in the left panels. The right panels show the related fluorescence spectra of fluorescein isothiocyanate (FITC) dextran (a) and Texas Red (b). All spectra are normalized, the one- and two-photon abscissa are aligned for equal transition energies. One and two-photon excitation spectra may differ considerably because of the converse selection

rules of the related absorption processes. The excitation wavelengths at $\lambda^{1P} = 488 \text{ nm}$ and 543 nm , as well as at $\lambda^{2P} = 800 \text{ nm}$ are accentuated by dotted vertical lines.

Figure 5: Multiphoton spectral imaging: (a) True color representation of a spectral image at $z = -21 \mu\text{m}$ with plots of the ROIs used for spectral analysis. (b) Fluorescence spectra series of ROI 1 showing the decline of Texas Red in the gel matrix (including particles). The Texas Red content in the particles is low and shows no clear trend as depicted in the series of the average spectra of 15 particles per image in (c). Since the Texas Red content of the particles does not change significantly, the decline of Texas Red in ROI 1 must occur in the gel matrix itself. The excitation power for the multiphoton spectral images was $P_{EX} = 15 \text{ mW}$, the pixel acquisition time $t_{Px} = 3.2 \mu\text{s}$.

Figure 6: Quantitative spectral analysis of the Texas Red concentration in different skin compartments. Scheme (a) shows the baselines and spectral positions used for calculating the emission ratios used to determine the relative contents of the drug-model Texas Red in the ROIs. Panels (b, c, d) display the temporal evolution of the emission ratios as a measure of Texas Red content in the ROIs. In ROI 2 the Texas Red emission at 612 nm is divided by the average keratin autofluorescence intensity at 500 nm and 525 nm because of the interference of the broad autofluorescence emission with noise effects around 500 nm .

Figure 7: Multitracking experiments: (a, b, c) $325 \times 325 \mu\text{m}^2$ combined optical sections in -6 , -16 and $-32 \mu\text{m}$ depth. (d) A detail image of particles and skin surface. Each panel consists of a multiphoton excited image (predominantly keratin autofluorescence and

fluorescein, grey-scale, top left image), a 488 nm excited image (fluorescein, green-scale, top right image) and a 543 nm excited image (Texas Red, orange-scale, bottom left image), as well as an overlay of which (bottom right image). The excitation powers for the optical sections in the multitasking study were $P_{EX}(800 \text{ nm}) = 10 \text{ mW}$, $P_{EX}(488 \text{ nm}) = 50 \mu\text{W}$ and $P_{EX}(543 \text{ nm}) = 36 \mu\text{W}$, the pixel acquisition time was always $t_{px} = 3.2 \mu\text{s}$.

Figure 8: xz-multitracking sections composed from a stack of xy-optical sections with $3 \mu\text{m}$ distance in between. This representation nicely reveals the penetration profiles of Texas red into the skin and the correlation of the penetration behavior with skin morphology. The color coding is in accordance with Figure 7.

Figure 9: (a) $2 \times 2 \mu\text{m}^2$ scanning force microscopy image of an air-dried aqueous suspension of the PLGA nanoparticles on a glass substrate. The image was acquired in the tapping mode, 0.2Hz scan speed. The topography from 180nm to 550nm altitude is encoded in the grey scale. (b) Histogram of the particle diameter d obtained by photocorrelation spectroscopy. The line is a Gaussian fit to the data.

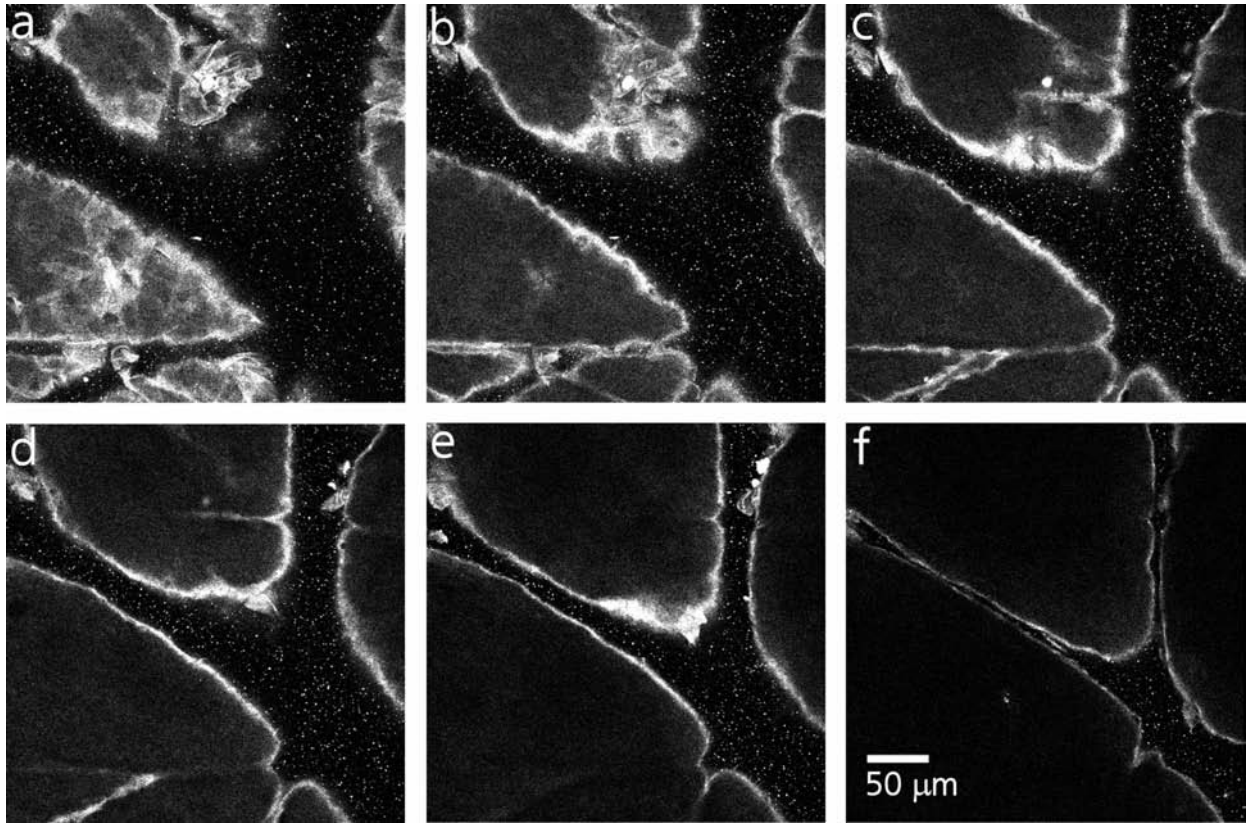


Figure 1: $325 \times 325 \mu\text{m}^2$ multiphoton optical sections of human skin treated with a hydrogel suspension of two color labeled nanoparticles. The sub-surface depths of the displayed images are (a) $-6\mu\text{m}$, (b) $-9\mu\text{m}$, (c) $-12\mu\text{m}$, (d) $-15\mu\text{m}$, (e) $-24\mu\text{m}$, (f) $-33\mu\text{m}$. The keratin autofluorescence clearly shows the surface of the dermatoglyphs. The excitation power for the multiphoton optical sections was $P_{\text{EX}} = 5 \text{ mW}$, the pixel acquisition time $t_{\text{px}} = 3.2 \mu\text{s}$.

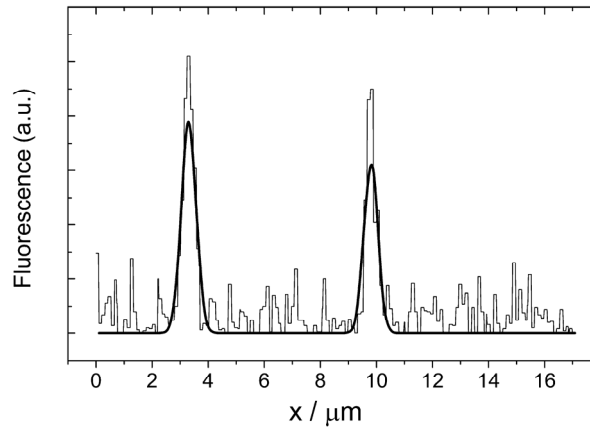


Figure 2: Fluorescence intensity profile of two multiphoton excited nanoparticles *in situ*. The bimodal fit yields a full width at half maximum (FWHM) of $0.5\mu\text{m}$. This is a reasonable value for the diffraction limited resolution of nanoscale particles under the present conditions.

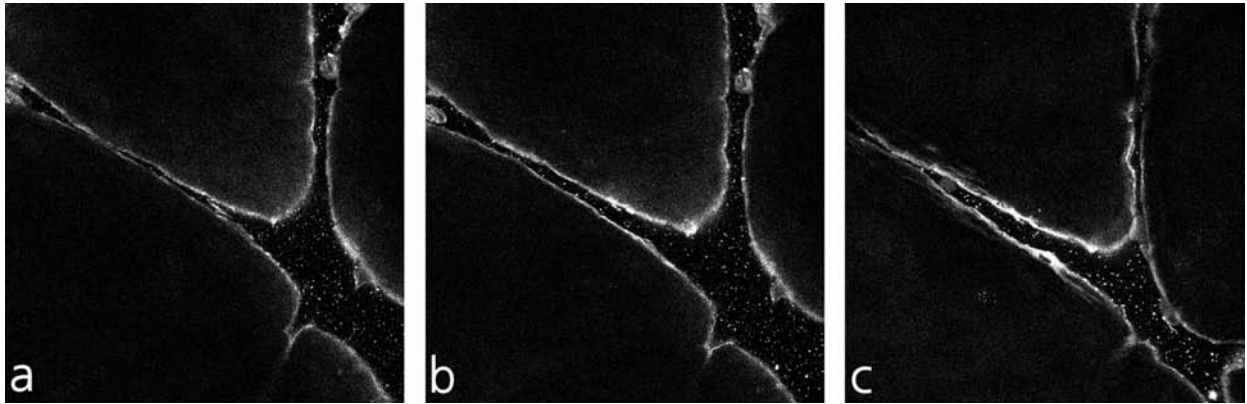


Figure 3: $325 \times 325 \mu\text{m}^2$ multiphoton optical sections at a depth of $-27\mu\text{m}$ 15, 50 and 315 minutes after application of the nanoparticulate formulation.

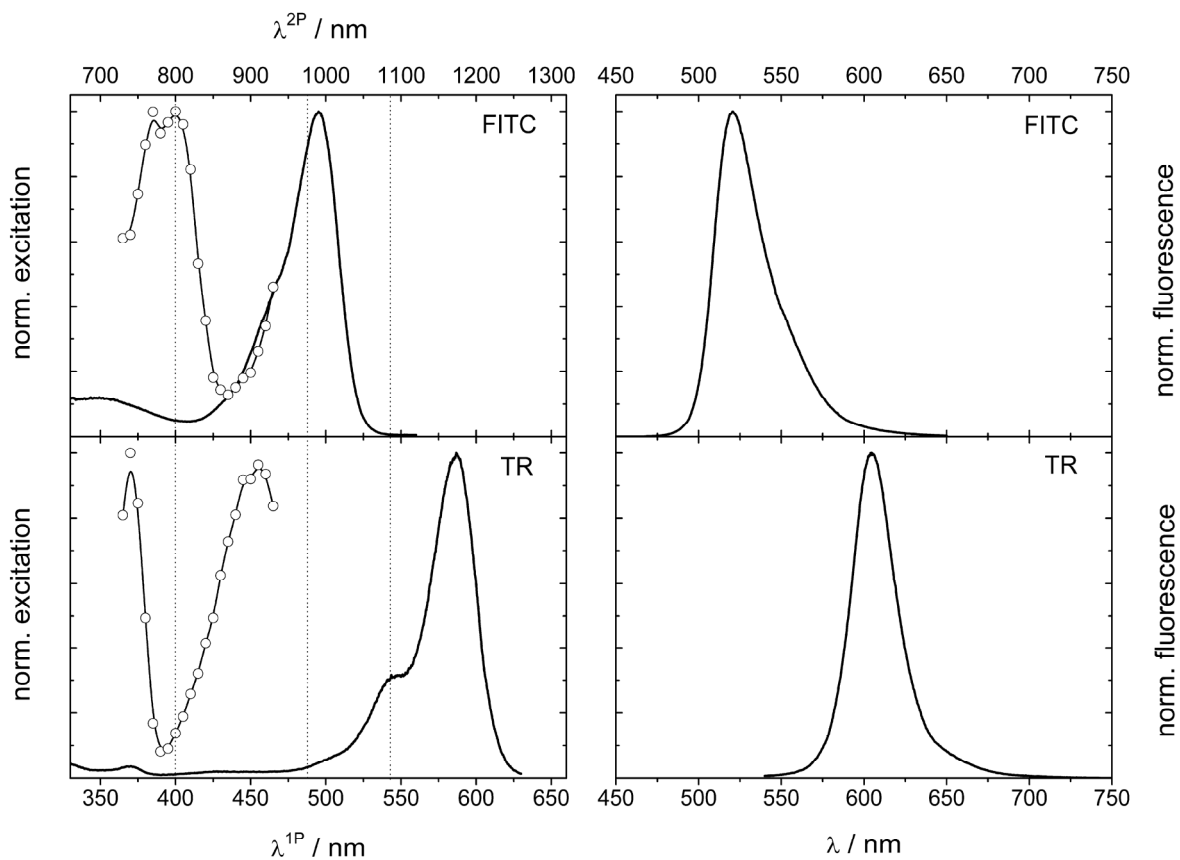


Figure 4: One- (solid line) and two-photon (open circles plus B-spline fit) excitation spectra are displayed in the left panels. The right panels show the related fluorescence spectra of fluorescein isothiocyanate (FITC) dextran (a) and Texas Red (b). All spectra are normalized, the one- and two-photon abscissa are aligned for equal transition energies. One and two-photon excitation spectra may differ considerably because of the converse selection rules of the related absorption processes. The excitation wavelengths at $\lambda^{1P} = 488 \text{ nm}$ and $\lambda^{2P} = 800 \text{ nm}$ are accentuated by dotted vertical lines.

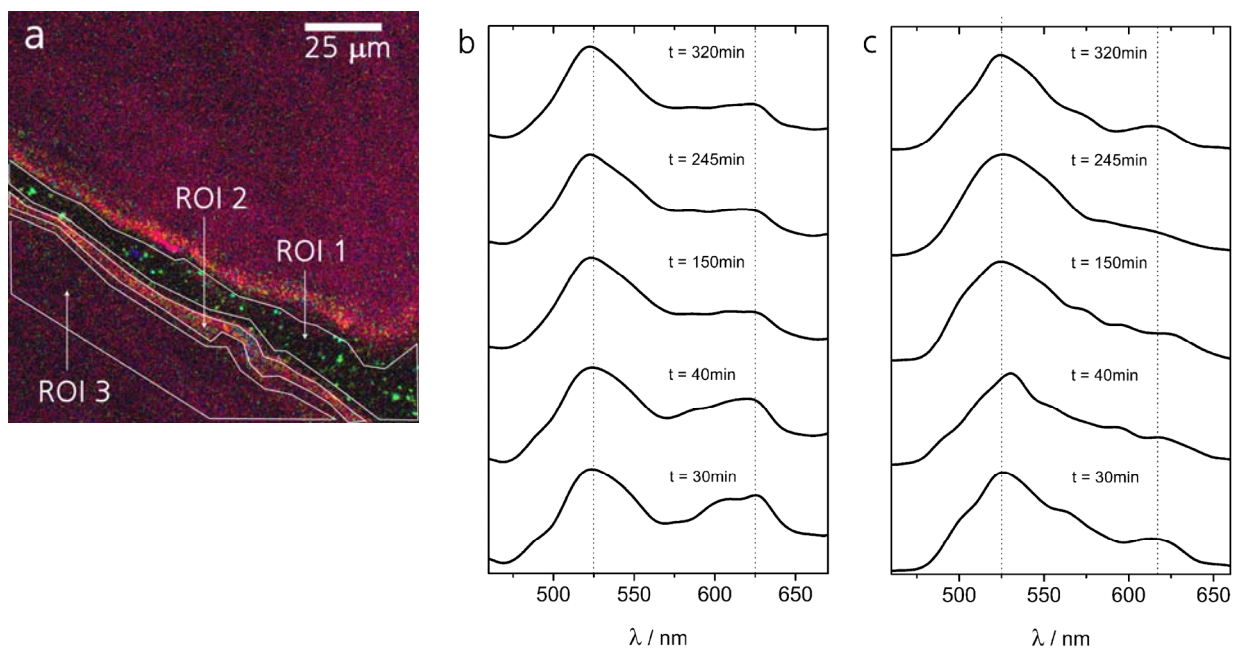


Figure 5: Multiphoton spectral imaging: (a) True color representation of a spectral image at $z = -21 \mu\text{m}$ with plots of the ROIs used for spectral analysis. (b) Fluorescence spectra series of ROI 1 showing the decline of Texas Red in the gel matrix (including particles). The Texas Red content in the particles is low and shows no clear trend as depicted in the series of the average spectra of 15 particles per image in (c). Since the Texas Red content of the particles does not change significantly, the decline of Texas Red in ROI 1 must occur in the gel matrix itself. The excitation power for the multiphoton spectral images was $P_{\text{EX}} = 15 \text{ mW}$, the pixel acquisition time $t_{\text{px}} = 3.2 \mu\text{s}$.

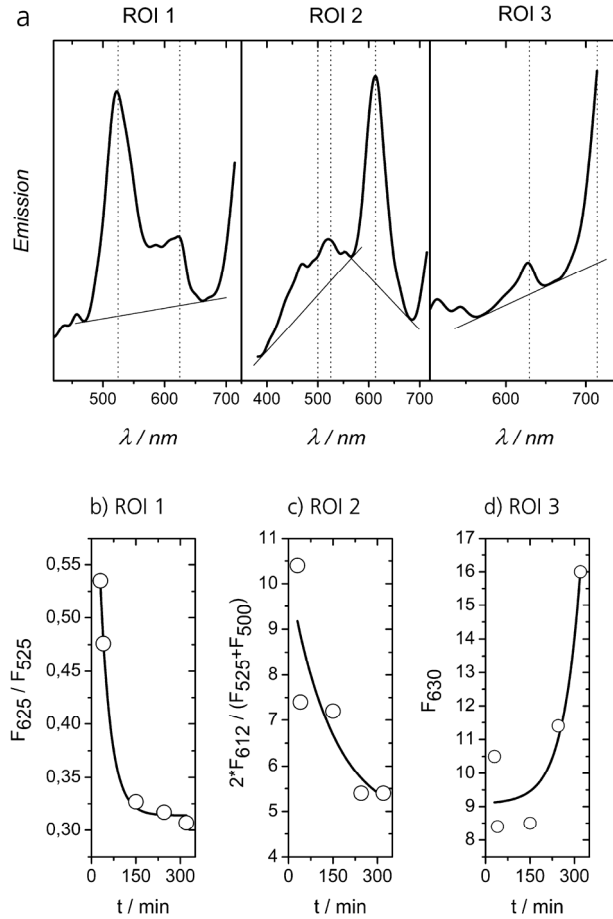


Figure 6: Quantitative spectral analysis of the Texas Red concentration in different skin compartments. Scheme (a) shows the baselines and spectral positions used for calculating the emission ratios used to determine the relative contents of the drug-model Texas Red in the ROIs. Panels (b, c, d) display the temporal evolution of the emission ratios as a measure of Texas Red content in the ROIs. In ROI 2 the Texas Red emission at 612 nm is divided by the average keratin autofluorescence intensity at 500 nm and 525 nm because of the interference of the broad autofluorescence emission with noise effects around 500 nm.

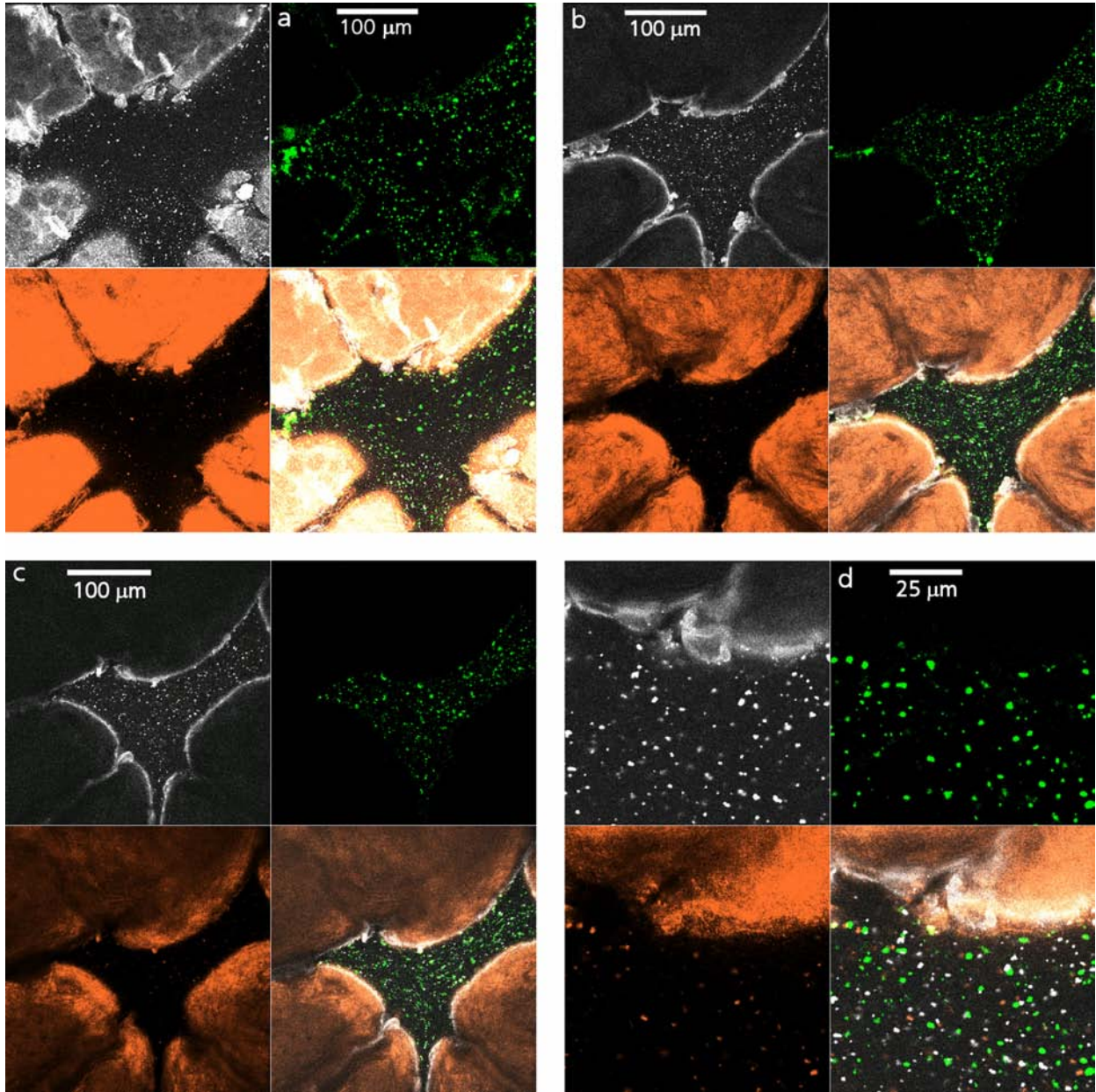


Figure 7: Multitracking experiments: (a, b, c) $325 \times 325 \mu\text{m}^2$ combined optical sections in -6 , -16 and $-32 \mu\text{m}$ depth. (d) A detail image of particles and skin surface. Each panel consists of a multiphoton excited image (predominantly keratin autofluorescence and fluorescein, grey-scale, top left image), a 488 nm excited image (fluorescein, green-scale, top right image) and a 543 nm excited image (Texas Red, orange-scale, bottom left image), as well as an overlay of which (bottom right image). The excitation powers for the optical sections in the multitracking study were $P_{\text{EX}}(800 \text{ nm}) = 10 \text{ mW}$, $P_{\text{EX}}(488 \text{ nm}) = 50 \mu\text{W}$ and $P_{\text{EX}}(543 \text{ nm}) = 36 \mu\text{W}$, the pixel acquisition time was always $t_{\text{PX}} = 3.2 \mu\text{s}$.

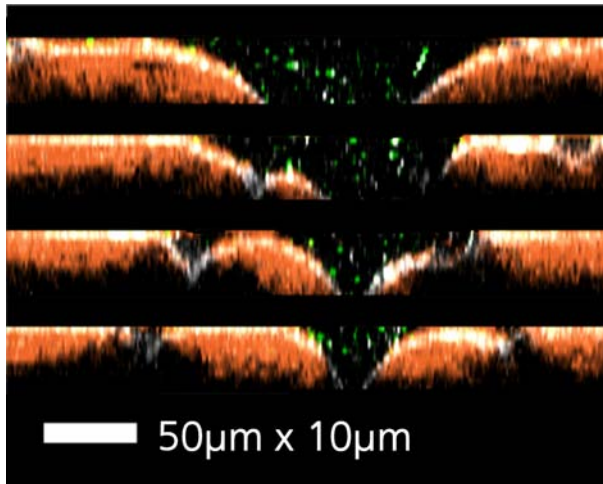


Figure 8: xz-multitracking sections composed from a stack of xy-optical sections with 3 µm distance in between. This representation nicely reveals the penetration profiles of Texas red into the skin and the correlation of the penetration behavior with skin morphology. The color coding is in accordance with Figure 7.

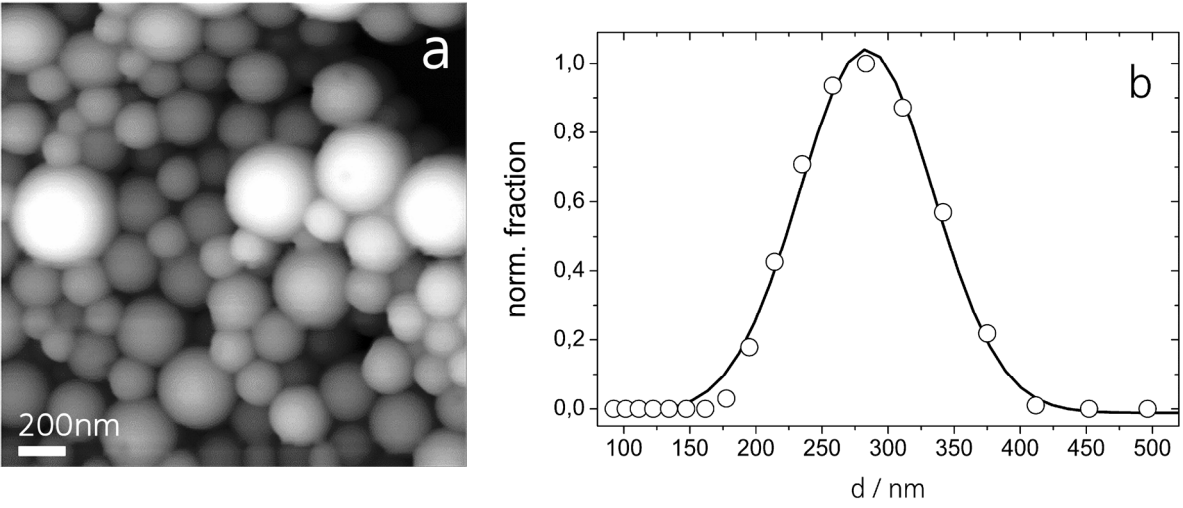


Figure 9: (a) $2 \times 2 \mu\text{m}^2$ scanning force microscopy image of an air-dried aqueous suspension of the PLGA nanoparticles on a glass substrate. The image was acquired in the tapping mode, 0.2 Hz scan speed. The topography from 180 nm to 550 nm altitude is encoded in the grey scale. (b) Histogram of the particle diameter d obtained by photocorrelation spectroscopy. The line is a Gaussian fit to the data.